NANO LETTERS

pubs.acs.org/NanoLett

Letter

Direct Observation of Spin−Orbit Interaction of Light via Chiroptical Responses

Jincheng Ni, Shunli Liu, Yang Chen, Guangwei Hu, Yanlei Hu, Weijin Chen, Jiawen Li, Jiaru Chu, Cheng-Wei Qiu,* and Dong Wu*

Cite This: *Nano Lett.* 2022, 22, 9013−9019

Read Online

ACCESS | Metrics & More | Article Recommendations | Supporting Information

ABSTRACT: The spin−orbit interaction of light is a fundamental manifestation of controlling its angular momenta with numerous applications in photonic spin Hall effects and chiral quantum optics. However, observation of an optical spin Hall effect, which is normally very weak with subwavelength displacements, needs quantum weak measurements or sophisticated metasurfaces. Here, we theoretically and experimentally demonstrate the spin−orbit interaction of light in the form of strong chiroptical responses by breaking the in-plane inversion symmetry of a dielectric substrate. The chiroptical signal is observed at the boundary of a microdisk illuminated by circularly polarized vortex beams at normal incidence. The generated chiroptical spectra are tunable for different photonic orbital angular momenta and microdisk diameters. Our findings, correlating photonic spin−orbit interaction with chiroptical responses, may provide a route for exploiting optical information processing, enantioselective sensing, and chiral metrology.

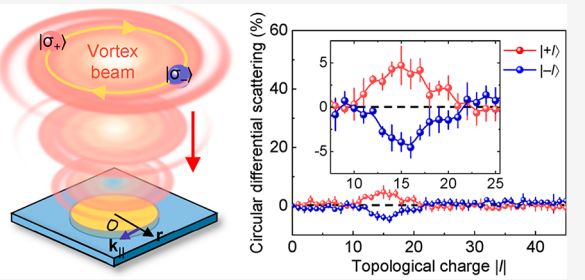

KEYWORDS: *spin−orbit interaction of light, spin Hall effect, orbital angular momentum, spin angular momentum, chiroptical response*

Recently, photonic angular momenta have been widely explored for controlling the spatial distributions of light.[1−4] The spin−orbit interaction of light (SOIL) demonstrates that the circularly polarized light with spin angular momentum (SAM) can affect and control the intensity distributions and propagation paths of light on an interface. Akin to semiconductor spintronics, the spin−orbit coupling effect with transverse spin-dependent displacement is also dubbed the photonic version of a spin Hall effect[5−9] or optical Rashba effect.[10] However, the optical spin Hall effect normally demonstrates subwavelength displacements on an air−dielectric interface by the transverse nature of photon polarization.[5,6] Therefore, the experimental measurements of such a small displacement largely rely on ultrasensitive quantum weak measurements,[5] accumulation of multiple reflections,[11] or enhancement with wavelength-scale plasmonic structures.[12−19]

Distinguished from the intrinsic SAM, the photonic orbital angular momentum (OAM) has both intrinsic and extrinsic terms. The latter is dependent on the trajectory of the light beam by propagating at a distance from the coordinate origin,[2,20] such as the phenomena of spin−orbit coupling in an optical spin Hall effect. The intrinsic OAM, hereafter referred as OAM, carried by optical vortices is reflected in the azimuthal phase distribution $\exp(il\varphi)$, where the integer l is the topological charge and its sign indicates the handedness of helical phase wavefront.[21−24] Vortex beams with theoretically unbounded OAM states have been widely applied in the fields of optical micromanipulation, chiroptical sensing, and optical information multiplexing.[22,25−27] In inhomogeneous media, the vortex beams carrying opposite topological charges also demonstrate distinct transverse deflections: namely, exhibiting the photonic orbital Hall effect.[28−30] Although vortex beams with high-order OAM states can significantly increase the angular momenta of photons, the observation of an orbital Hall effect, like its spin counterpart, still needs to distinguish wavelength-scale shifts.[29]

Chiroptical responses, utilizing photonic SAM or OAM, can collect the chiroptical signals in materials with high sensitivity by chiral light−matter interactions.[31−33] For example, circular dichroism (CD) spectroscopy, characterized by the differential absorption between right- and left-handed circularly polarized light, has been successfully applied in distinguishing the chirality of molecules or nanostructures.[34−38] For achiral nanoholes, CD signals can be also achieved by oblique incidence[39] or an SAM-to-OAM transformation.[36] However,

Received: August 17, 2022
Revised: October 29, 2022
Published: November 3, 2022

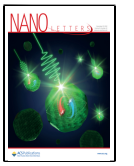

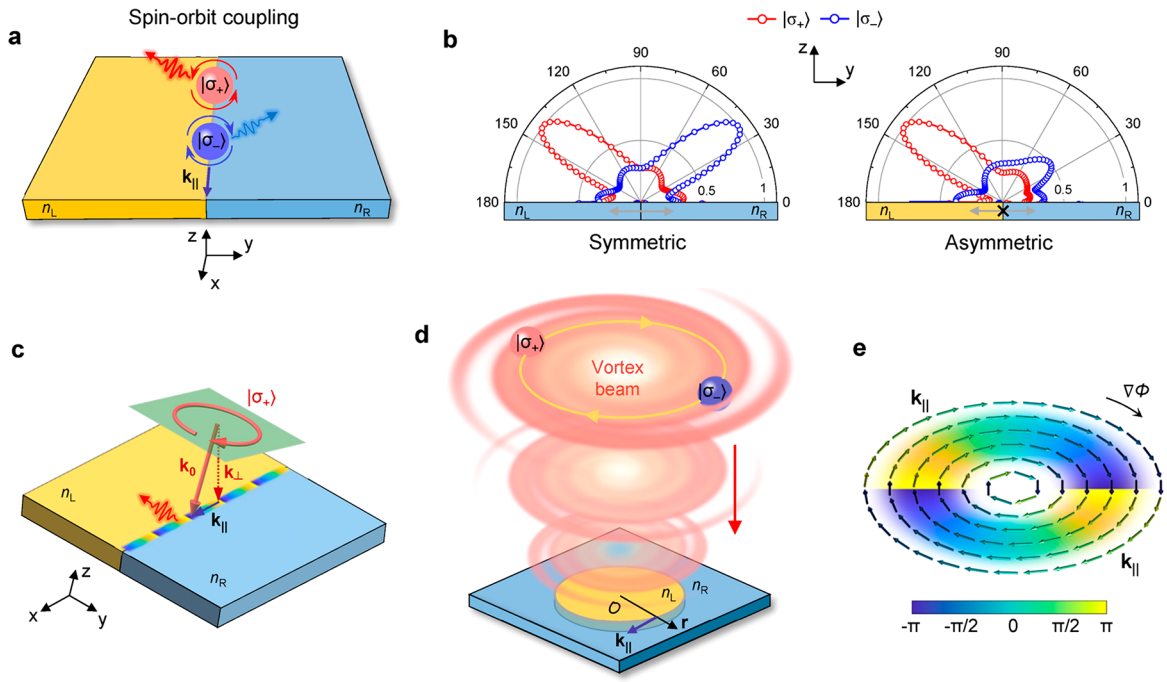

Figure 1. Concept of chiroptical signals induced by spin−orbit interactions of light. (a) Schematic of $|\sigma_\pm\rangle$ circularly polarized dipoles oscillating on an air−dielectric interface, leading to unidirectional scattering distribution. The in-plane pseudo-wavevector $\mathbf{k}_{\parallel}$ propagates along the boundary (y = 0). The refractive indices of $y < 0$ and $y > 0$ dielectric parts are n_L and n_R, respectively. (b) Simulated angle-resolved scattering intensity of $|\sigma_\pm\rangle$ circularly polarized dipoles on the symmetric (left panel: $n_L = n_R = 3$) and asymmetric (right panel: $n_L = 4.5$, $n_R = 1.5$) interface. The symmetry of scattering intensity between $|\sigma_\pm\rangle$ states is broken on the asymmetric surface, resulting in chiroptical responses. (c) The in-plane pseudowavevector $\mathbf{k}_{\parallel}$ can be provided by a plane wave under oblique incidence. (d) Schematic of circularly polarized vortex beams incident on a dielectric disk, where the rectilinear boundary is changed into a circular one. (e) The vortex beam has an azimuthal phase gradient, providing the in-plane pseudo-wavevector $\mathbf{k}_{\parallel}$.

the observation of spin−orbit coupling in the spin Hall effect with sensitive chiroptical spectroscopy remains elusive.

Here, we theoretically predict and experimentally validate the spin−orbit coupling in the form of chiroptical signals. As shown in Figure 1a, electromagnetic waves induced by circularly polarized dipoles on an air−dielectric interface propagate along a given direction instead of the opposite direction, resulting in the spin−orbit coupling. In the y−z plane, two circularly polarized dipoles $|\sigma_\pm\rangle = (\hat{y} \pm i\hat{z})/\sqrt{2}$ predominately radiate to scatter in opposite directions, yielding different scattering intensity distributions for $y < 0$ and $y > 0$ sections (Figure 1b). However, the total scattering intensities are equal due to the spatial symmetry of the dielectric substrate. By changing their refractive indices ($n_L \neq n_R$), we can break the in-plane inversion symmetry of the dielectric substrate. For $n_L > n_R$, the total scattering intensity of the $|\sigma_+\rangle$ dipole substantially exceeds that with the $|\sigma_-\rangle$ dipole, resulting in chiroptical responses. The sign of the chiroptical signal is flipped for $n_L < n_R$ (see Figures S1 and S2 for more discussions).

To sustain the surface-propagating mode and circular dipoles in the y−z plane, the in-plane wavevector $\mathbf{k}_{\parallel}$ on the air−dielectric interface is typically provided by an oblique plane wave, as shown in Figure 1c. Instead of the rectilinear boundary, we further consider a circular boundary of a dielectric disk with diameter D. In this scenario, we can introduce OAM beams to provide the in-plane wavevector $\mathbf{k}_{\parallel}$ along the circular boundary, as shown in Figure 1d. The vortex beam has an azimuthal phase gradient $\nabla\Phi = l/r \cdot \hat{\mathbf{e}}_\varphi$, where φ is the azimuthal angle and $\hat{\mathbf{e}}_\varphi$ is a unit vector pointing along the cylindrical coordinate direction (Figure 1e). When the vortex beam impinges on the interface, the helical phase wavefront introduces an in-plane pseudo-wavevector $\mathbf{k}_{\parallel} = l/r \cdot \hat{\mathbf{k}}_\perp \times \hat{\mathbf{r}}$, where $\mathbf{k}_\perp$ is the axial wavevector component. As a result, the spin−orbit coupling in the form of a chiroptical response is expected to be probed on the circular boundary at normal incidence (see Section S3 and Figure S3 for more details).

To experimentally verify our predictions, circularly polarized vortex beams with tunable topological charges are focused on a microdisk. For simplicity, we choose an air−dielectric boundary (n_L = 1.51, n_R = 1), where the chiroptical response can still exist on the boundary (see Figure S1). Figure 2a shows the experimental configuration for probing spin−orbit coupling effects. A phase-only spatial light modulator (SLM) is used for generating vortex beams with tunable topological charges. The microdisk with a height of 2 μm and a diameter of 10.6 μm is fabricated by two-photon direct laser writing in a photopolymer material, as shown in Figure 2b. The reflected light can be collected by a charge-coupled device (CCD) camera (see Section S1 for more experimental details).

In our experiments, we detect the reflection on the microdisk by circularly polarized vortex beams with different topological charges. In Figure 2c, a pronounced valley is shown in the reflectance spectrum for topological charges in the range of 10−25, where a microcavity resonance is excited by illuminating the boundary of the microdisk (see Section S4 for more details). Remarkably, different reflectance can be observed at the valleys for opposite spin states. To be more specific, the reflectance with $|\sigma_+\rangle$ spin state is larger than that with $|\sigma_-\rangle$ in the valley region. In contrast, the reflectance with $|\sigma_+\rangle$ is smaller than that with $|\sigma_-\rangle$ for topological charge $|-l\rangle$, as

https://doi.org/10.1021/acs.nanolett.2c03266
Nano Lett. 2022, 22, 9013−9019

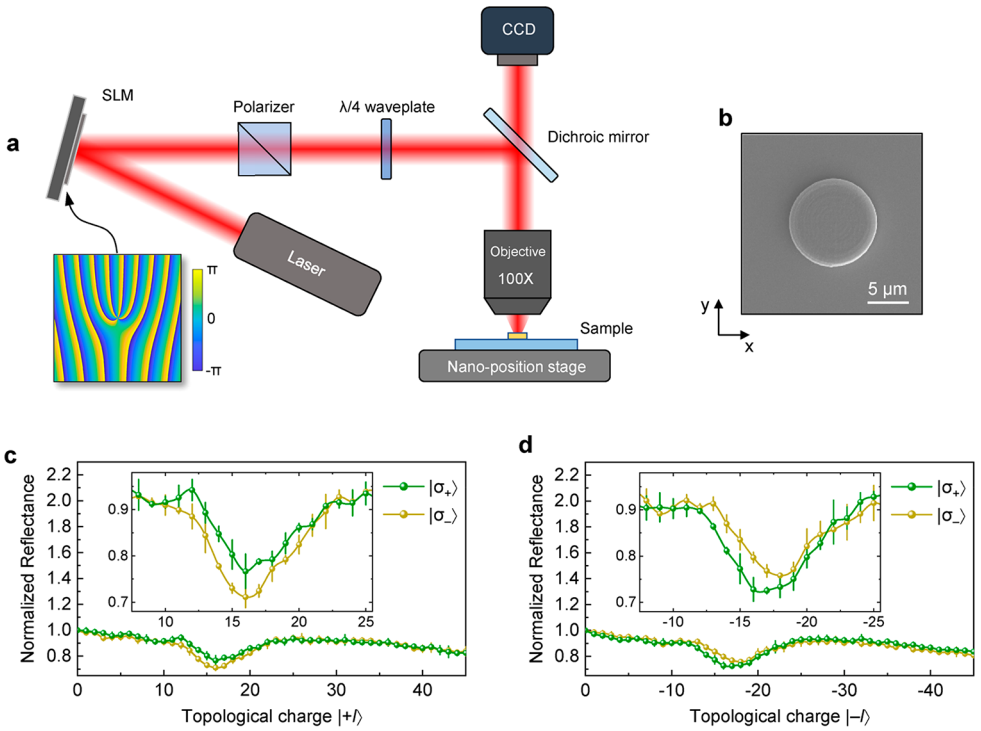

Figure 2. Experimental demonstration on microdisks by circularly polarized vortex beams. (a) Optical setup. The Gaussian beam is modulated to linearly polarized vortex beams with controllable topological charge l by fork holograms. Then the vortex beam is tailored to $|\sigma_+\rangle$ or $|\sigma_-\rangle$ circular polarization by a polarizer and quarter-wave plate. Finally, the modulated circularly polarized vortex beam is focused on the microdisk by an optical microscope system. The inset shows the fork hologram with topological charge $l = 4$. (b) Scanning electron micrograph (SEM) image of the engineered microdisk. (c, d) Normalized reflectance of circularly polarized vortex beams as a function of topological charge $|+l\rangle$ (c) and $|-l\rangle$ (d). Each curve is the average of multiple measurements shown as the mean value and standard deviation of the mean.

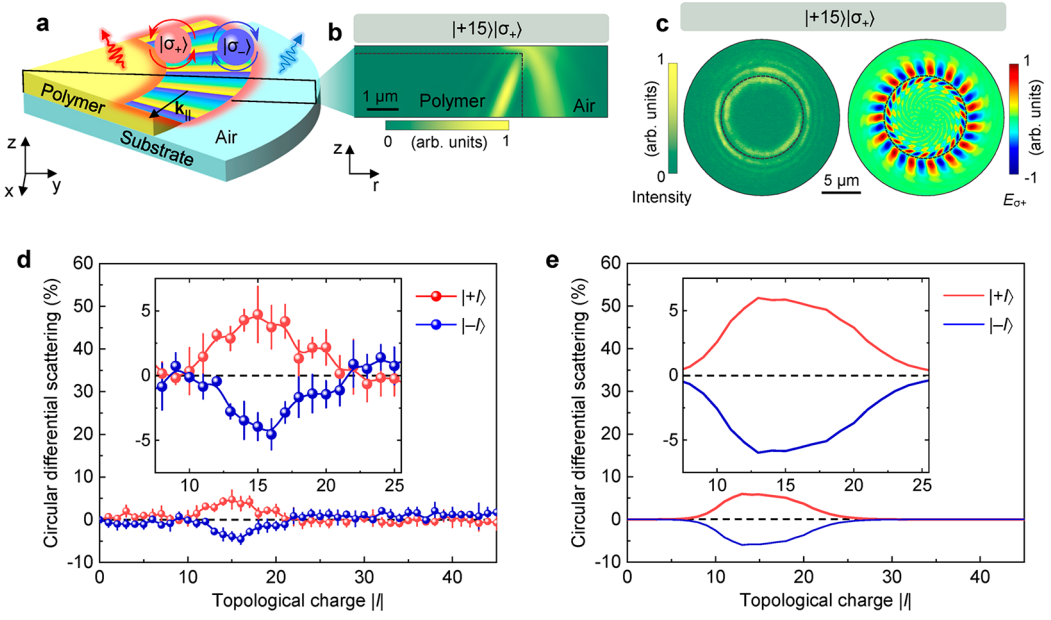

Figure 3. Simulated demonstrations and CDS spectra in angular momentum space. (a) Sectorial schematic of the circularly polarized vortex beam impinging on the boundary of a microdisk. Both the vortex beam and microdisk are cylindrically symmetrical by aligning their axes. (b) Simulated cross-sectional intensity distribution of the microdisk illuminated by a $|\sigma_+\rangle$ circularly polarized vortex beam with topological charge $|+15\rangle$. (c) Measured optical intensity (left panel) and simulated $E_{\sigma+}$ mode (right panel) profiles on the microdisk by the $|+15\rangle|\sigma_+\rangle$ vortex beam. Dashed lines indicate the position of the microdisk. (d, e) Measured (d) and simulated (e) CDS spectra as a function of topological charge $|l|$ on the achiral microdisk.

shown in Figure 2d. The chiral electromagnetic wave under time reversal switches its propagation direction, which results in the inversion of photonic chirality on the transverse plane.[40−42] The intrinsic angular momentum of light $|\pm l\rangle|\sigma_\pm\rangle$ can be transformed into $|\mp l\rangle|\sigma_\mp\rangle$ in free space: that is, $|\pm l\rangle \rightarrow |\mp l\rangle$ and $|\sigma_\pm\rangle \rightarrow |\sigma_\mp\rangle$ by time-reversal symmetry breaking.

https://doi.org/10.1021/acs.nanolett.2c03266
Nano Lett. 2022, 22, 9013−9019

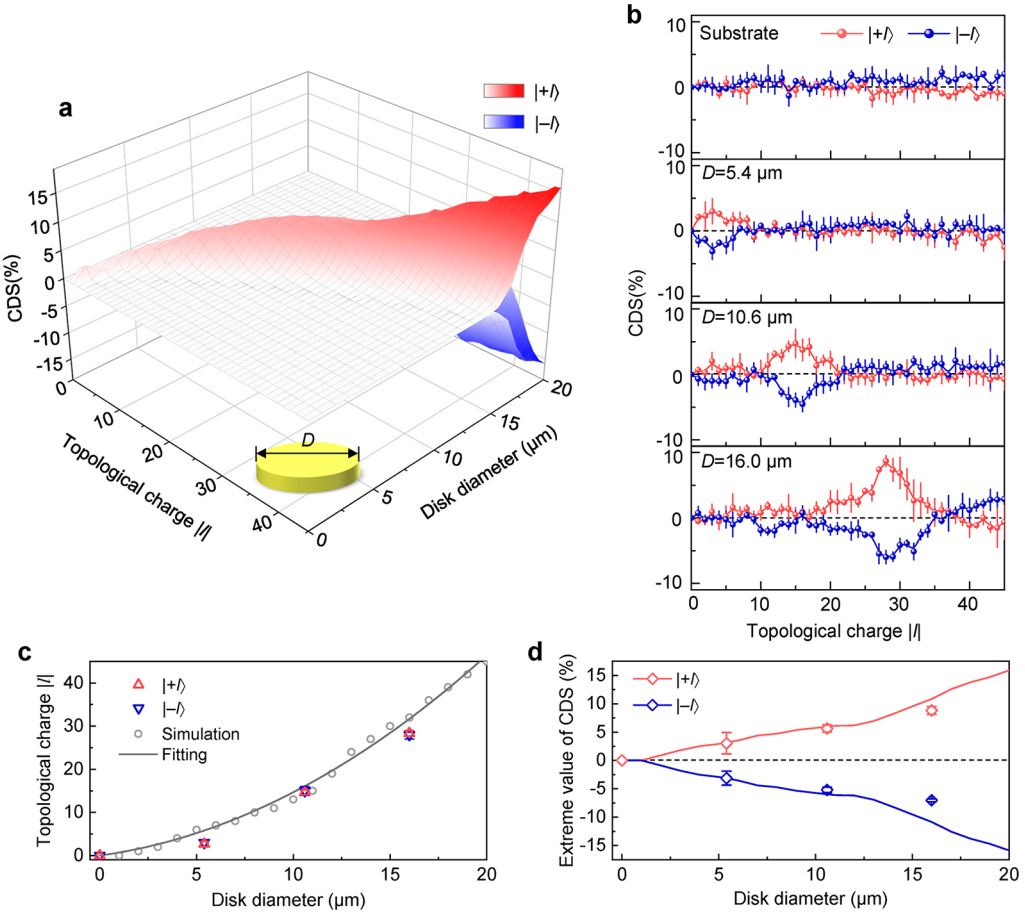

Figure 4. Chiroptical properties on varying microdisk diameters. (a) 3D mapping graph of simulated CDS spectra related to topological charge $|l|$ and microdisk diameters. (b) Measured CDS spectra for varying microdisks (diameters: 5.4, 10.6, and 16.0 μm). The top CDS spectrum indicates the sample without a microdisk. (c) The corresponding topological charge $|\pm l\rangle$ of peaks or valleys on CDS spectra for varying microdisk diameters. The gray dots and line indicate the simulated data and theoretical analysis, respectively. (d) Experimental (dots) and simulated (lines) dependences of the extreme CDS values on the microdisk diameters.

Given that spin−orbit coupling is dependent on the signs of both spin states and in-plane pseudo-wavevector $\mathbf{k}_{||}$, which is determined by the topological charge $|\pm l\rangle$, the total system shows time-reversal invariant by inversing the signs of σ and l simultaneously (see Figure S4). Therefore, the characteristics of reflectance spectra with topological charge $|-l\rangle$ are theoretically inverse to the situation with $|+l\rangle$, which is confirmed in the experimental results.

Recently, the chiroptical signals have been reported by transferring SAM to OAM under a high-numerical-aperture (NA) objective lens, which demonstrates SAM-dependent intensity distributions on the focal plane.[36,43,44] To decrease the SAM-to-OAM transformation, we focus the circularly polarized vortex beams by an objective lens with NA = 0.9 in our experiments. The residual cross-polarization transformation (<3%) can be neglected without obvious influences on our experimental results (see Figures S6 and S7 for more discussions). To further understand the phenomena, the interaction between photonic angular momenta and the microdisk is investigated by a full-wave simulation with a finite-difference time-domain (FDTD) method. We analyze the vortex beam exactly impinging on the boundary of the microdisk (Figure 3a). In this scenario, the intrinsic angular momenta of vortex beams can strikingly affect the electric field distribution on the achiral microdisk by spin−orbit coupling. Due to the diffraction effect on the boundary, the donut-shaped vortex beam is split into two ring distributions. Presented in the cross-sectional intensity distribution on the $r-z$ plane, one branch propagates into the microdisk and the other propagates into air (Figure 3b). The spin-dependent scattering appears by matching the vortex beam and microdisk diameter, which is also proved by the optical images of the CCD camera (Figure 3c). The transverse electric field demonstrates azimuthal distributions by the excitation of vortex beams (see Figures S8 and S9).

To establish the relationship of such propagation-direction-dependent or chiral light−matter interactions with photonic SAM and OAM, we compare the reflectance spectra for generating chiroptical signals. The reflectance difference between opposite spin states can be defined as circular differential scattering (CDS)

$$\mathrm{CDS}^{l} = \frac{I^{l}_{\sigma_+} - I^{l}_{\sigma_-}}{I^{l}_{\sigma_+} + I^{l}_{\sigma_-}} \tag{1}$$

where I_{σ_+} and I_{σ_-} are the reflectance of vortex beams with $|\sigma_+\rangle$ and $|\sigma_-\rangle$ spin states, respectively. As shown in Figure 3d, one can find that a strong CDS is located in the range of $10 \leq |l| \leq 25$, where vortex beams illuminate on the boundary of the microdisk. The following characteristic features on CDS

https://doi.org/10.1021/acs.nanolett.2c03266
Nano Lett. 2022, 22, 9013−9019

spectra can also be observed in our experiments. First, no obvious CDS signal is observed by illuminating on the sample away from boundary area ($|l| < 10$ or $|l| > 25$). Second, the CDS spectra of circularly polarized vortex beams are mirror-symmetric for $CDS^{l} = -CDS^{-l}$ with respect to the zero line. Third, distinguished from traditional chiroptical phenomena caused by chiral materials, the chiroptical signals on achiral microdisks are induced by the intrinsic chirality of light. The simulated CDS spectra are in good agreement with the experimental measurements (Figure 3e). Due to the orthogonality between SAM and OAM, the CDS spectra can be also defined as the chiroptical signals between $|+l\rangle$ and $|-l\rangle$ vortex beams.

To investigate the robustness of chiroptical responses, we further analyze microdisks with different diameters. The simulated results demonstrate robust mirror-symmetric CDS values for vortex beams with opposite topological charge $|\pm l\rangle$, as shown in Figure 4a. The sign of CDS is exclusively determined by the topological charges and is independent of the microdisk diameters. By varying the microdisk diameter from 5.4 to 16.0 μm, the mirror-symmetric property of CDS spectra is also confirmed in our experiments (Figure 4b). As a control sample, no remarkable chiroptical signal is observed on the substrate without a microdisk.

In our experiment, the microdisks are located at the defocused plane of objective, where the diameter of vortex beam is proportional to $\sqrt{|l|}$.[45] As the chiroptical signals are generated at the boundaries of microdisks, the extreme CDS values can be achieved by vortex beams with topological charge $|l| = \alpha D^2$, where the constant α is dependent on the experimental configurations (Figure 4c). By tailoring the microdisk diameters, a strong CDS signal can be induced by spin−orbit coupling, as shown in Figure 4d. The simulated extreme CDS values for different microdisk diameters are in good agreement with the measured results. The small deviations for larger microdisk diameters can be attributed to the radiation leakages at the edge of the CCD and the defective fabrication of microdisks. Moreover, the extreme values of CDS spectra could be further increased by tuning the refractive indices of dielectric materials to improve the asymmetric distributions beside the boundary. The proposed chiroptical properties provide a versatile method to probe the spin−orbit coupling effect for different structural and material parameters.

In conclusion, we have proposed a scheme to measure the spin−orbit coupling effect by chiroptical signals. The tunable chiroptical responses are experimentally observed on the microdisks by circularly polarized vortex beams. Our method, combining the intrinsic photonic angular momenta (SAM and OAM), is convenient and versatile to allow the realization of the spin−orbit coupling effect even at normal incidence. Moreover, the adjustability of photonic angular momenta can be predominantly improved by introducing theoretically unbounded topological charges of vortex beams. The sensitive chiroptical spectroscopy technique makes it possible to quantify the inherent spin-dependent scattering of light−matter interactions, opening doors to further understand and control spin−orbit coupling effects, as well as the connections between spin−orbit coupling and chiroptical responses. The sensitivity of chiroptical signals can be further increased by orders of magnitude for precision metrology, by commercial CD instruments that are widely used for probing chiral molecules or nanostructures. Moreover, we may extend the concept from a single microdisk to a large array of microdisks to achieve strong coupling between incident vortex beams and the microdisks with small beam divergence.[46] This work, utilizing variable superposition of SAM and OAM, may find applications in spin-based nano-optics and next-generation chiroptical spectroscopy.[47] In addition, we expect that the strong chiroptical responses generated by spin−orbit coupling effects can provide a new physical insight into the origin of chiroptical activity.

■ ASSOCIATED CONTENT

Supporting Information

The Supporting Information is available free of charge at https://pubs.acs.org/doi/10.1021/acs.nanolett.2c03266.

Materials and methods, near-field unidirectional scattering of circularly polarized dipoles, reflectance difference on the interface by circularly polarized light, whispering-gallery modes in the microdisk resonator, comparison with SAM-to-OAM transformation mechanism, and analysis of CDS with total angular momentum conservation (PDF)

■ AUTHOR INFORMATION

Corresponding Authors

Cheng-Wei Qiu − *Department of Electrical and Computer Engineering, National University of Singapore, Singapore 117583, Singapore;* orcid.org/0000-0002-6605-500X; Email: chengwei.qiu@nus.edu.sg

Dong Wu − *CAS Key Laboratory of Mechanical Behavior and Design of Materials, Department of Precision Machinery and Precision Instrumentation, University of Science and Technology of China, Hefei, Anhui 230027, People's Republic of China;* orcid.org/0000-0003-0623-1515; Email: dongwu@ustc.edu.cn

Authors

Jincheng Ni − *Department of Electrical and Computer Engineering, National University of Singapore, Singapore 117583, Singapore;* orcid.org/0000-0001-9308-4511

Shunli Liu − *CAS Key Laboratory of Mechanical Behavior and Design of Materials, Department of Precision Machinery and Precision Instrumentation, University of Science and Technology of China, Hefei, Anhui 230027, People's Republic of China*

Yang Chen − *CAS Key Laboratory of Mechanical Behavior and Design of Materials, Department of Precision Machinery and Precision Instrumentation, University of Science and Technology of China, Hefei, Anhui 230027, People's Republic of China;* orcid.org/0000-0002-8501-5417

Guangwei Hu − *Department of Electrical and Computer Engineering, National University of Singapore, Singapore 117583, Singapore;* orcid.org/0000-0002-3023-9632

Yanlei Hu − *CAS Key Laboratory of Mechanical Behavior and Design of Materials, Department of Precision Machinery and Precision Instrumentation, University of Science and Technology of China, Hefei, Anhui 230027, People's Republic of China;* orcid.org/0000-0003-1964-0043

Weijin Chen − *Department of Electrical and Computer Engineering, National University of Singapore, Singapore 117583, Singapore*

Jiawen Li − *CAS Key Laboratory of Mechanical Behavior and Design of Materials, Department of Precision Machinery and Precision Instrumentation, University of Science and*

https://doi.org/10.1021/acs.nanolett.2c03266
Nano Lett. 2022, 22, 9013−9019

Technology of China, Hefei, Anhui 230027, People's Republic of China; orcid.org/0000-0003-3950-6212

Jiaru Chu − *CAS Key Laboratory of Mechanical Behavior and Design of Materials, Department of Precision Machinery and Precision Instrumentation, University of Science and Technology of China, Hefei, Anhui 230027, People's Republic of China;* orcid.org/0000-0001-6472-8103

Complete contact information is available at: https://pubs.acs.org/10.1021/acs.nanolett.2c03266

Author Contributions

J.N. and C.-W.Q. conceived the idea and developed the theory. J.N., Y.C., and G.H. performed the simulations. J.N. and S.L. performed the experiments. J.N., J.L., D.W., J.C., and Y.H. analyzed the data. J.N., C.-W.Q., and D.W. wrote the manuscript. C.-W.Q. and D.W. supervised the project. All authors discussed the results and commented on the manuscript.

Notes

The authors declare no competing financial interest.

■ ACKNOWLEDGMENTS

We acknowledge financial support from the National Natural Science Foundation of China (Grant Nos. 51875544, 51805509, 91963127, 61805230, and 51675503), the USTC Research Funds of the Double First-Class Initiative (Grant No. YD2090002005), the National Key R&D Program of China (Grant No. 2018YFB1105400), and the Foundation of Equipment Development Department (Grant No. 6140922010901). The authors thank the USTC Center for Micro and Nanoscale Research and Fabrication. G.H. acknowledges support from A*STAR AME Young Individual Research Grants (YIRG, No. A2084c0172). C.-W.Q. is supported by the National Research Foundation, Prime Minister's Office, Singapore, under Competitive Research Program Award NRF-CRP22-2019-0006.

■ REFERENCES

(1) Araneda, G.; Walser, S.; Colombe, Y.; Higginbottom, D. B.; Volz, J.; Blatt, R.; Rauschenbeutel, A. Wavelength-scale errors in optical localization due to spin−orbit coupling of light. *Nat. Phys.* **2019**, *15*, 17−21.

(2) Bliokh, K. Y.; Rodriguez-Fortuno, F. J.; Nori, F.; Zayats, A. V. Spin-orbit interactions of light. *Nat. Photonics* **2015**, *9*, 796−808.

(3) Fang, Y.; Han, M.; Ge, P.; Guo, Z.; Yu, X.; Deng, Y.; Wu, C.; Gong, Q.; Liu, Y. Photoelectronic mapping of the spin−orbit interaction of intense light fields. *Nat. Photonics* **2021**, *15*, 115−120.

(4) Zhang, Z.; Qiao, X.; Midya, B.; Liu, K.; Sun, J.; Wu, T.; Liu, W.; Agarwal, R.; Jornet, J. M.; Longhi, S.; et al. Tunable topological charge vortex microlaser. *Science* **2020**, *368*, 760−763.

(5) Hosten, O.; Kwiat, P. Observation of the spin Hall effect of light via weak measurements. *Science* **2008**, *319*, 787−790.

(6) Yin, X.; Ye, Z.; Rho, J.; Wang, Y.; Zhang, X. Photonic spin Hall effect at metasurfaces. *Science* **2013**, *339*, 1405−1407.

(7) Dai, H.; Yuan, L.; Yin, C.; Cao, Z.; Chen, X. Direct Visualizing the Spin Hall Effect of Light via Ultrahigh-Order Modes. *Phys. Rev. Lett.* **2020**, *124*, No. 053902.

(8) Bliokh, K. Y.; Smirnova, D.; Nori, F. Quantum spin Hall effect of light. *Science* **2015**, *348*, 1448−1451.

(9) Gong, S.-H.; Alpeggiani, F.; Sciacca, B.; Garnett, E. C.; Kuipers, L. Nanoscale chiral valley-photon interface through optical spin-orbit coupling. *Science* **2018**, *359*, 443−447.

(10) High, A. A.; Devlin, R. C.; Dibos, A.; Polking, M.; Wild, D. S.; Perczel, J.; de Leon, N. P.; Lukin, M. D.; Park, H. Visible-frequency hyperbolic metasurface. *Nature* **2015**, *522*, 192−196.

(11) Bliokh, K. Y.; Niv, A.; Kleiner, V.; Hasman, E. Geometrodynamics of spinning light. *Nat. Photonics* **2008**, *2*, 748.

(12) O'connor, D.; Ginzburg, P.; Rodríguez-Fortuño, F. J.; Wurtz, G. A.; Zayats, A. V. Spin−orbit coupling in surface plasmon scattering by nanostructures. *Nat. Commun.* **2014**, *5*, 5327.

(13) Rodríguez-Fortuño, F. J.; Marino, G.; Ginzburg, P.; O'Connor, D.; Martínez, A.; Wurtz, G. A.; Zayats, A. V. Near-field interference for the unidirectional excitation of electromagnetic guided modes. *Science* **2013**, *340*, 328−330.

(14) Peng, L.; Duan, L.; Wang, K.; Gao, F.; Zhang, L.; Wang, G.; Yang, Y.; Chen, H.; Zhang, S. Transverse photon spin of bulk electromagnetic waves in bianisotropic media. *Nat. Photonics* **2019**, *13*, 878−882.

(15) Barik, S.; Karasahin, A.; Flower, C.; Cai, T.; Miyake, H.; DeGottardi, W.; Hafezi, M.; Waks, E. A topological quantum optics interface. *Science* **2018**, *359*, 666−668.

(16) Parappurath, N.; Alpeggiani, F.; Kuipers, L.; Verhagen, E. Direct observation of topological edge states in silicon photonic crystals: Spin, dispersion, and chiral routing. *Sci. Adv.* **2020**, *6*, eaaw4137.

(17) Hu, G.; Hong, X.; Wang, K.; Wu, J.; Xu, H.-X.; Zhao, W.; Liu, W.; Zhang, S.; Garcia-Vidal, F.; Wang, B.; et al. Coherent steering of nonlinear chiral valley photons with a synthetic Au−WS_2 metasurface. *Nat. Photonics* **2019**, *13*, 467−472.

(18) Söllner, I.; Mahmoodian, S.; Hansen, S. L.; Midolo, L.; Javadi, A.; Kiršanskė, G.; Pregnolato, T.; El-Ella, H.; Lee, E. H.; Song, J. D.; et al. Deterministic photon−emitter coupling in chiral photonic circuits. *Nat. Nanotechnol.* **2015**, *10*, 775−778.

(19) Sun, L.; Wang, C.-Y.; Krasnok, A.; Choi, J.; Shi, J.; Gomez-Diaz, J. S.; Zepeda, A.; Gwo, S.; Shih, C.-K.; Alù, A.; et al. Separation of valley excitons in a MoS_2 monolayer using a subwavelength asymmetric groove array. *Nat. Photonics* **2019**, *13*, 180−184.

(20) O'Neil, A. T.; MacVicar, I.; Allen, L.; Padgett, M. J. Intrinsic and extrinsic nature of the orbital angular momentum of a light beam. *Phys. Rev. Lett.* **2002**, *88*, No. 053601.

(21) Allen, L.; Beijersbergen, M. W.; Spreeuw, R. J. C.; Woerdman, J. P. Orbital angular-momentum of light and the transformation of Laguerre-Gaussian laser modes. *Phys. Rev. A* **1992**, *45*, 8185−8189.

(22) Ni, J.; Huang, C.; Zhou, L.-M.; Gu, M.; Song, Q.; Kivshar, Y.; Qiu, C.-W. Multidimensional phase singularities in nanophotonics. *Science* **2021**, *374*, eabj0039.

(23) Jin, Z.; Janoschka, D.; Deng, J.; Ge, L.; Dreher, P.; Frank, B.; Hu, G.; Ni, J.; Yang, Y.; Li, J.; et al. Phyllotaxis-inspired nanosieves with multiplexed orbital angular momentum. *eLight* **2021**, *1*, 5.

(24) Bao, Y.; Ni, J.; Qiu, C. W. A minimalist single-layer metasurface for arbitrary and full control of vector vortex beams. *Adv. Mater.* **2020**, *32*, 1905659.

(25) Ouyang, X.; Xu, Y.; Xian, M.; Feng, Z.; Zhu, L.; Cao, Y.; Lan, S.; Guan, B.-O.; Qiu, C.-W.; Gu, M.; et al. Synthetic helical dichroism for six-dimensional optical orbital angular momentum multiplexing. *Nat. Photonics* **2021**, *15*, 901−907.

(26) Liu, S.; Ni, J.; Zhang, C.; Wang, X.; Cao, Y.; Wang, D.; Ji, S.; Pan, D.; Li, R.; Wu, H.; et al. Tailoring Optical Vortical Dichroism with Stereometamaterials. *Laser Photon. Rev.* **2022**, *16*, 2100518.

(27) Liu, J.; Shi, M.; Chen, Z.; Wang, S.; Wang, Z.; Zhu, S. Quantum photonics based on metasurfaces. *Opto-Electronic Advances* **2021**, *4*, No. 200092.

(28) Bliokh, K. Y. Geometrical optics of beams with vortices: Berry phase and orbital angular momentum Hall effect. *Phys. Rev. Lett.* **2006**, *97*, No. 043901.

(29) Dennis, M. R.; Götte, J. B. Topological aberration of optical vortex beams: determining dielectric interfaces by optical singularity shifts. *Phys. Rev. Lett.* **2012**, *109*, 183903.

(30) Zhang, M.; Ren, H.; Ouyang, X.; Jiang, M.; Lu, Y.; Hu, Y.; Fu, S.; Li, Z.; Chen, Z.; Guan, B.-O.; et al. Nanointerferometric

Discrimination of the Spin−Orbit Hall Effect. *ACS Photon.* **2021**, *8*, 1169−1174.
(31) Kuzyk, A.; Schreiber, R.; Fan, Z. Y.; Pardatscher, G.; Roller, E. M.; Hogele, A.; Simmel, F. C.; Govorov, A. O.; Liedl, T. DNA-based self-assembly of chiral plasmonic nanostructures with tailored optical response. *Nature* **2012**, *483*, 311−314.
(32) Ni, J.; Liu, S.; Hu, G.; Hu, Y.; Lao, Z.; Li, J.; Zhang, Q.; Wu, D.; Dong, S.; Chu, J. Giant helical dichroism of single chiral nanostructures with photonic orbital angular momentum. *ACS Nano* **2021**, *15*, 2893−2900.
(33) Kuzyk, A.; Schreiber, R.; Zhang, H.; Govorov, A. O.; Liedl, T.; Liu, N. Reconfigurable 3D plasmonic metamolecules. *Nat. Mater.* **2014**, *13*, 862−866.
(34) Lee, H. E.; Ahn, H. Y.; Mun, J.; Lee, Y. Y.; Kim, M.; Cho, N. H.; Chang, K.; Kim, W. S.; Rho, J.; Nam, K. T. Amino-acid- and peptide-directed synthesis of chiral plasmonic gold nanoparticles. *Nature* **2018**, *556*, 360−365.
(35) Ni, J.; Liu, S.; Wu, D.; Lao, Z.; Wang, Z.; Huang, K.; Ji, S.; Li, J.; Huang, Z.; Xiong, Q.; et al. Gigantic vortical differential scattering as a monochromatic probe for multiscale chiral structures. *Proc. Natl. Acad. Sci. U. S. A.* **2021**, *118*, No. e2020055118.
(36) Zambrana-Puyalto, X.; Vidal, X.; Molina-Terriza, G. Angular momentum-induced circular dichroism in non-chiral nanostructures. *Nat. Commun.* **2014**, *5*, 4922.
(37) Ávalos-Ovando, O.; Besteiro, L. V.; Movsesyan, A.; Markovich, G.; Liedl, T.; Martens, K.; Wang, Z.; Correa-Duarte, M. A.; Govorov, A. O. Chiral Photomelting of DNA-Nanocrystal Assemblies Utilizing Plasmonic Photoheating. *Nano Lett.* **2021**, *21*, 7298−7308.
(38) Zhang, S.; Park, Y.-S.; Li, J.; Lu, X.; Zhang, W.; Zhang, X. Negative refractive index in chiral metamaterials. *Phys. Rev. Lett.* **2009**, *102*, No. 023901.
(39) Maoz, B. M.; Ben Moshe, A.; Vestler, D.; Bar-Elli, O.; Markovich, G. Chiroptical Effects in Planar Achiral Plasmonic Oriented Nanohole Arrays. *Nano Lett.* **2012**, *12*, 2357−2361.
(40) Marrucci, L.; Manzo, C.; Paparo, D. Optical spin-to-orbital angular momentum conversion in inhomogeneous anisotropic media. *Phys. Rev. Lett.* **2006**, *96*, 163905.
(41) Carlon Zambon, N.; St-Jean, P.; Milicevic, M.; Lemaitre, A.; Harouri, A.; Le Gratiet, L.; Bleu, O.; Solnyshkov, D. D.; Malpuech, G.; Sagnes, I.; Ravets, S.; Amo, A.; Bloch, J. Optically controlling the emission chirality of microlasers. *Nat. Photonics* **2019**, *13*, 283−288.
(42) Rechcińska, K.; Król, M.; Mazur, R.; Morawiak, P.; Mirek, R.; Łempicka, K.; Bardyszewski, W.; Matuszewski, M.; Kula, P.; Piecek, W.; et al. Engineering spin-orbit synthetic Hamiltonians in liquid-crystal optical cavities. *Science* **2019**, *366*, 727−730.
(43) Zhao, Y. Q.; Edgar, J. S.; Jeffries, G. D. M.; McGloin, D.; Chiu, D. T. Spin-to-orbital angular momentum conversion in a strongly focused optical beam. *Phys. Rev. Lett.* **2007**, *99*, No. 073901.
(44) Du, L.; Yang, A.; Zayats, A. V.; Yuan, X. Deep-subwavelength features of photonic skyrmions in a confined electromagnetic field with orbital angular momentum. *Nat. Phys.* **2019**, *15*, 650−654.
(45) Padgett, M. J.; Miatto, F. M.; Lavery, M. P. J.; Zeilinger, A.; Boyd, R. W. Divergence of an orbital-angular-momentum-carrying beam upon propagation. *New J. Phys.* **2015**, *17*, No. 023011.
(46) Qiao, X.; Midya, B.; Gao, Z.; Zhang, Z.; Zhao, H.; Wu, T.; Yim, J.; Agarwal, R.; Litchinitser, N. M.; Feng, L. Higher-dimensional supersymmetric microlaser arrays. *Science* **2021**, *372*, 403−408.
(47) Ye, L.; Yang, L.; Zheng, X.; Mukamel, S. Enhancing Circular Dichroism Signals with Vector Beams. *Phys. Rev. Lett.* **2021**, *126*, 123001.

https://doi.org/10.1021/acs.nanolett.2c03266
Nano Lett. 2022, 22, 9013−9019